Instrument Science Report WFC3 2008-22

WFC3 TV3 Testing: UVIS-1′ and IR-4 Noise Trends

A.R. Martel
August 19, 2008

ABSTRACT

We examine the read noise of the flight UVIS-1′ detector of the Wide Field Camera 3 during its third thermal vacuum campaign at the Goddard Space Flight Center. Only the frames acquired at the default gain of 1.5 e^-/DN and four amplifier readout (ABCD) are considered. The read noise at a temperature of -82 C and for no on-chip binning, calculated from the pairwise subtraction of bias frames, is 3.03 ± 0.04, 3.13 ± 0.01, 3.08 ± 0.02, and 3.18 ± 0.01 e^- for amplifiers A, B, C, and D, respectively. At binnings of 2x2 and 3x3, the noise is higher by up to 10%. Amplifier D has the highest read noise for all binnings. The read noise calculated from the serial virtual overscan correlates with the level of the imaging area - the pairwise subtraction of bias frames is therefore the preferable method for estimating the read noise. The CEI specification of a read noise of < 4 e^- is easily met for an operating detector temperature of less than -20 C. There is no difference in the read noise between MEBs 1 and 2. A superbias frame shows no weak odd/even effect in any quadrant. We also investigate the overall noise trends of the flight IR-4 detector for the RAPID and SPARS25 sampling sequences. The CDS noise on MEB2 is lower than on MEB1. The largest difference is about 0.8 e^- in quadrant 4. Quadrants 2 and 3 are the least noisy for MEB2 and MEB1, respectively.

Operated by the Association of Universities for Research in Astronomy, Inc., for the National Aeronautics and Space Administration

Introduction

The Wide Field Camera 3 (WFC3) underwent its third and final thermal vacuum campaign (TV3) in the Space Environment Simulator (SES) at the Goddard Space Flight Center from Feb 20, 2008 (day of year 51) to Apr 21, 2008 (day of year 112). The corresponding ID numbers of the frames in the WFC3 ground database are 48658 to 59262. For this report, we have assembled a sample of frames to calculate the read noise of the four amplifiers of the flight detectors UVIS-1′ (CCD18 - amplifiers C and D, CCD178 - amplifiers A and B) and IR-4 (FPA165). We treat only the frames with the default on-orbit readout mode : four amplifiers (ABCD) and standard gains of 1.5 e^-/DN for the UVIS and 2.5 e^-/DN for the IR.

Prior efforts to characterize the read noise of the WFC3 UVIS detector have been documented in Baggett & Hilbert (2004; UVIS-1/ambient), Hilbert & Baggett (2004; UVIS-1/ambient), Hilbert & Baggett (2005; UVIS-1/TV1), Baggett (2007; UVIS-2/ambient), and Martel (2007; UVIS-2/TV2). Similarly, noise analyses for the IR channel have been presented in Hilbert (2005; IR-2/TV1), Hilbert (2008a; IR-1/TV2), and most recently, Hilbert (2008b; IR-4/TV3). In the following, we present our sample choice, our method of analysis, and our results for the TV3 campaign.

Data

1. UVIS

For this study of the read noise of the CCDs of the WFC3 UVIS-1′ detector, we consider all the frames acquired in the default on-orbit configuration : a four amplifier readout (ABCD) and a gain of 1.5 e^-/DN. The frames span the entire duration of the TV3 campaign, which was bracketed by the Servicing Mission Functional Test in ambient conditions after the instrument was moved into the SES and by the UVIS Science Monitor (SMS UV28S04) before it was removed.

Several images had to be rejected. Some were taken in special modes, such as EPER to measure the CTE (SMS UV02S01A; Apr 10, 2008), that produced non-standard image dimensions and overscan regions. Saturated images, primarily flat fields, were also excluded as well as the post-flash image 48725 (Feb 22, 2008). Others were simply missing from the database while several possess corrupted FITS headers, sometimes resulting from a glitch in the data dump or from a mismatched CASTLE stimulus file. The final tally consists of 1088 frames with a binning of 1x1. Of these, 172 (16%) are bias frames as identified with the IQDETSEL keyword in the database.

The images were acquired over a range of detector temperatures, as defined by the IUVDETMP keyword; this permits a characterization of the temperature dependence of

the noise. In Fig. 1, we plot the histogram of the temperature distribution for all the frames (1x1 binning). The majority of the data was acquired at a temperature near the nominal on-orbit operating temperature of -83 C : there are 889 frames in the main peak at -82 C and of these, 127 are biases. Additionally, a search of the database yields 34 and 74 bias frames with on-chip binnings of 2x2 and 3x3, respectively, at -82 C. In the following, we will also separate the sample by instrument side or Main Electronics Box (MEB 1 or 2), to determine if one side generates more noise than the other in either detector.

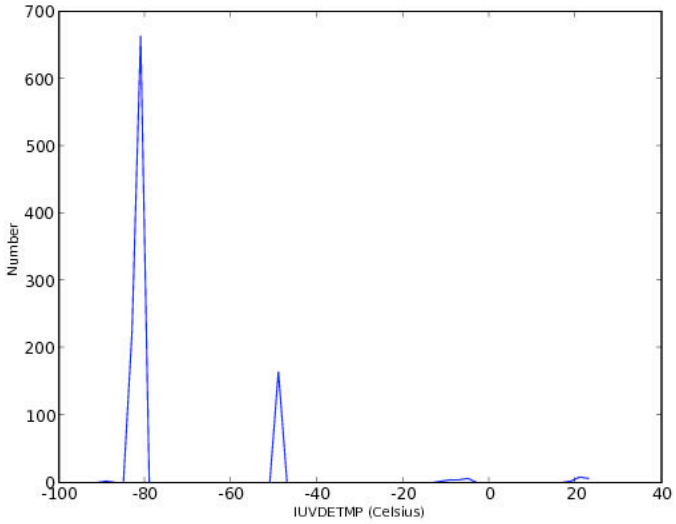

Figure 1 : Temperature distribution of all the UVIS-1′ frames acquired in TV3 in the standard mode (ABCD readout, gain=1.5, and 1x1 binning).

2. IR

For the analysis of the IR noise, all the dark frames acquired with the RAPID, 16-read sequence are considered. The RAPID sequence provides the fastest possible sampling (total integration time of 44 sec) and hence minimizes the accumulation of dark current between the non-destructive reads, thus in principle producing the most accurate noise values of all the available sequences. The majority of these frames were taken near the expected on-orbit operating setpoint of 145 K (-128 C); the temperature distribution, as defined with the IRFPATMP keyword, varies from 141 K to 147 K and peaks around 144 K (-129 C). The final sample consists of 92 RAPID frames at these temperatures.

We complement this sample with the comparatively large number (359 frames) of cold SPARS25 darks (16 reads; 353 sec), most of which served to monitor the bias jumps in the second quadrant of the detector throughout the campaign (SMSs IR01S03, IR01S10, and IR24S02). These will act mostly as a comparison sample and to confirm any trends seen in the RAPID dataset. We note that in this report, we are only concerned with general trends in the IR noise; a thorough analysis is presented in Hilbert (2008b).

Analysis

For both channels, all images were processed with a Python class specifically written to process the ground WFC3 data (Martel 2008). For the UVIS, we compare two common methods for calculating the noise in CCDs : 1) the standard deviation (divided by $\sqrt{2}$) in the imaging area of the pairwise subtraction of bias frames. Pairwise subtraction of bias frames removes any 2-dimensional gradient across the frame, leaving only the noise as residual. The biases are paired consecutively at the same temperature but with no overlap to insure independent measurements. This results in 63, 17, and 37 individual noise values for binnings of 1x1, 2x2, and 3x3, respectively. Gaussian fits to the histograms of the noise values yield the read noise as the location of the peak and its uncertainty as the standard deviation. 2) the RMS noise in the overscan region (in our case, the serial virtual overscan). As we will see below, the noise in the overscan area correlates slightly with the level in the imaging area and so we will concentrate on the bias frame overscans, which possess the lowest counts.

For the IR, an average of the vertical reference area is first subtracted from each read in the RAPID or SPARS25 sample sequence. Consecutive reads along the IR ramp image are then subtracted pairwise and an array of the standard deviations of the residuals is created. The distribution of these standard deviations does not exactly obey a Gaussian profile, especially in the wings. The noise, chosen as the location of the peak of the distribution, was therefore determined with a second-order polynomial. The uncertainty was still estimated with the standard deviation of a Gaussian fit. The fit can be made down to a specified level of the peak of the distribution; the upper 20% produces good results. Finally, for each quadrant (and each sampling sequence), the histogram of the noise values was fitted with a Gaussian.

This method of estimating the noise is the most common for multiple-read detectors; the result is called the Correlated Double Sampling (CDS) noise. The read noise itself is then the CDS noise divided by $\sqrt{2}$. Another noise measure is the effective noise which, in the read noise limited regime and for N reads uniformly sampled along the sequence, as for the RAPID and SPARS25 sequences, is given by the read noise multiplied by the factor $\sqrt{(12*N/(N-1)^2)}$ (Robberto 2007a). In this report, we only quote the standard CDS noise.

The counts or digital numbers (DNs) are translated to e^- with the gains tabulated in Baggett (2008) for the UVIS and with a gain of 2.26 e^-/DN for all four amplifiers of the IR detector (Hilbert 2008b).

Results

1. UVIS

1.1 Read Noise at -82 C

The distributions of the read noise calculated from the pairwise subtraction of the bias frames are shown in Fig. 2. The values are listed in Table 1 as well as those for binnings of 2x2 and 3x3, also calculated in the same manner. The average read noises are 3.10 e^-, 3.30 e^-, and 3.36 e^- for the respective binnings. There is a general trend for the binned data to have a higher read noise than the non-binned data, up to about 10% between the 1x1 and 3x3 binnings. The read noise from the virtual overscan (binning of 1x1) is also tabulated for comparison. In all cases, amplifier D has the highest read noise.

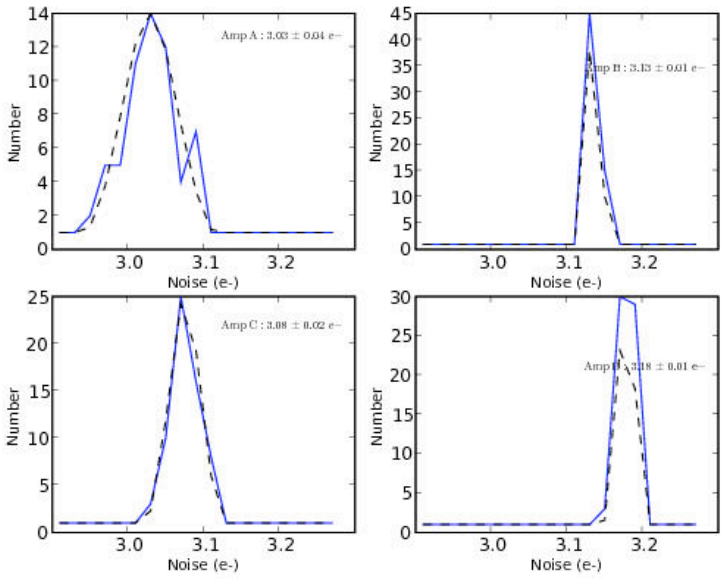

Figure 2 : Histograms of the read noise calculated from the pairwise subtraction of bias frames in the standard configuration (ABCD readout, gain=1.5, and no binning). The dashed line is a Gaussian fit.

Table 1 : Read Noise of the UVIS-1′ Detector in Standard Readout Mode at -82 C

Method	A	B	C	D
Bias Pairs (1x1)	3.03 ± 0.04	3.13 ± 0.01	3.08 ± 0.02	3.18 ± 0.01
Overscan (1x1)	3.12 ± 0.03	3.12 ± 0.02	3.05 ± 0.02	3.28 ± 0.02
Bias Pairs (2x2)	3.29 ± 0.03	3.28 ± 0.01	3.17 ± 0.03	3.46 ± 0.02
Bias Pairs (3x3)	3.37 ± 0.02	3.38 ± 0.01	3.18 ± 0.03	3.50 ± 0.02

1.2 Temperature Dependence

The temperature dependence of the read noise calculated from the overscan region of the bias frames is shown in Fig. 3. The Contract-End-Item specification 4.6.3 of a read noise less than 4 e^- is met for temperatures colder than about -20 C but the goal of 3 e^- is not satisfied.

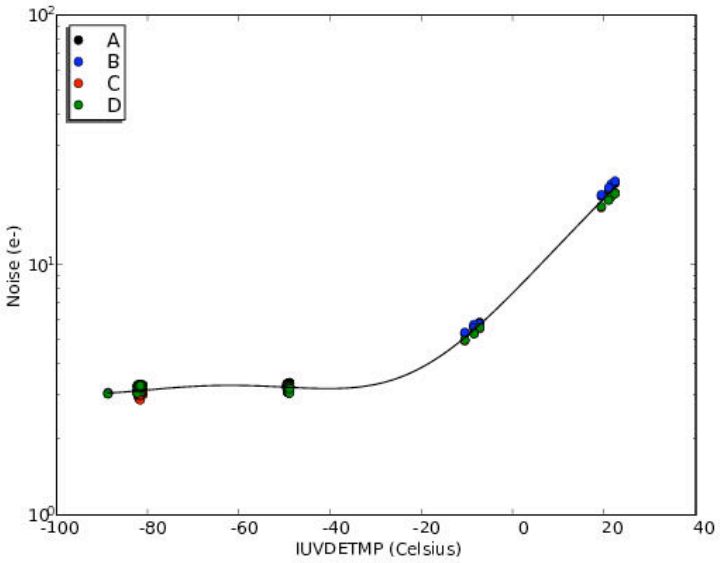

Figure 3 : Temperature dependence of the read noise of all the bias frames in standard configuration (ABCD readout, gain=1.5, and no binning). The solid line is a 4th-order polynomial fit to the combined data points.

1.3 Stability of the Read Noise at -82 C

In Fig. 4, we plot the read noise calculated from the overscan region of the bias frames as a function of the day the frame was obtained. After day 104, the instrument was configured to ambient environment in the SES and the temperature of the UVIS detector was raised to -49 C, hence the lack of data points past that day. Although there are gaps in the time sampling, reflecting the variety of activities over such a long campaign, we find no long-term trends in the behavior of the read noise for any of the amplifiers. In particular, there are no obvious differences in the noise between the MEBs except perhaps for a slight drop around day 100 on MEB2. The noise is well constrained within a band of 3.0 e^- to 3.3 e^-.

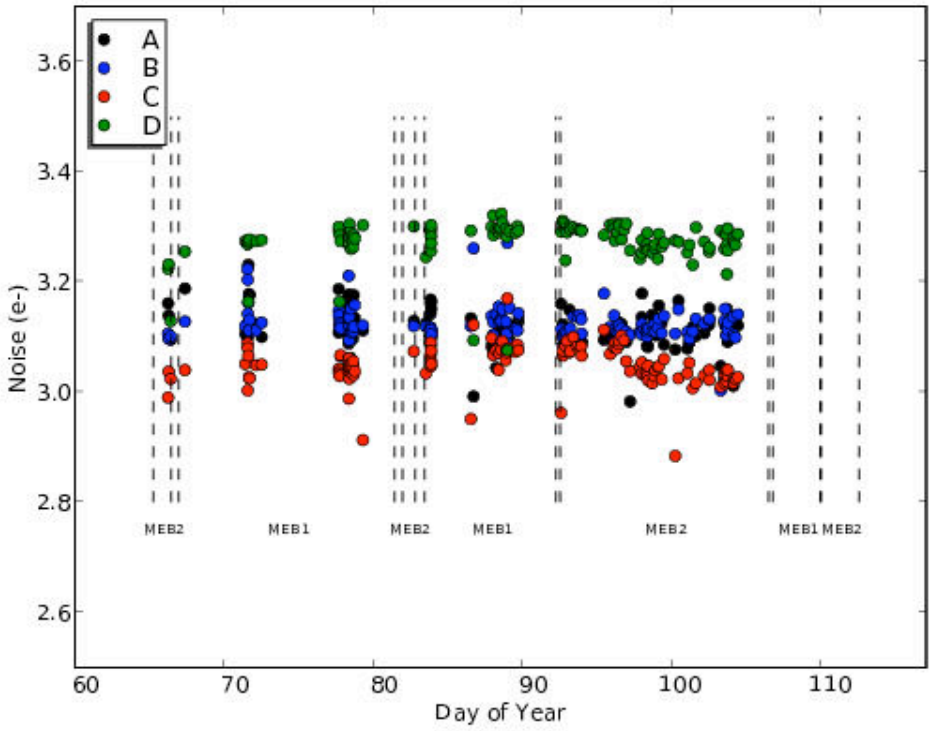

Figure 4 : The read noise of the bias frames at -82 C as a function of the day in TV3.

1.4 Overscan Noise Dependence on Imaging Area Levels

In Martel (2007), for the UVIS-2 detector, the read noise measured from the serial virtual overscan was found to correlate with the level in the imaging area. Here, we verify if this also holds true for UVIS-1′. In Fig.5, the read noise of each amplifier is plotted against the median level of its imaging area. The median level is calculated in a 1000x1000 box centered on each quadrant to avoid any possible edge effects. The large

cluster of data points between 40000 e^- and 50000 e^- results from an intensive series of flat fields acquired near the end of the campaign to populate the pipeline reference files.

There appears to be a change in the read noise around an imaging level of 30000 e^-. Below this value, the sequence of the amplifiers in order of decreasing noise is : D, A, B, and C. But above this value, the order changes to : B, D, C, A. Hence, B and C have more noise at higher counts while A and D show a drop in noise. We note that the change in the read noise over the full range of the imaging area (5000 e^- to 60000 e^-, say) is relatively small, ~0.1 e^- or 5%. The observed correlations could be due to a non-perfect serial transfer of the accumulated charge, resulting in a 'leak' between the imaging area and the serial virtual overscan region (e.g. Robberto 2007b). Noise measurements from the serial virtual overscan are therefore not ideal for this detector - the pairwise subtraction of bias frames is preferable.

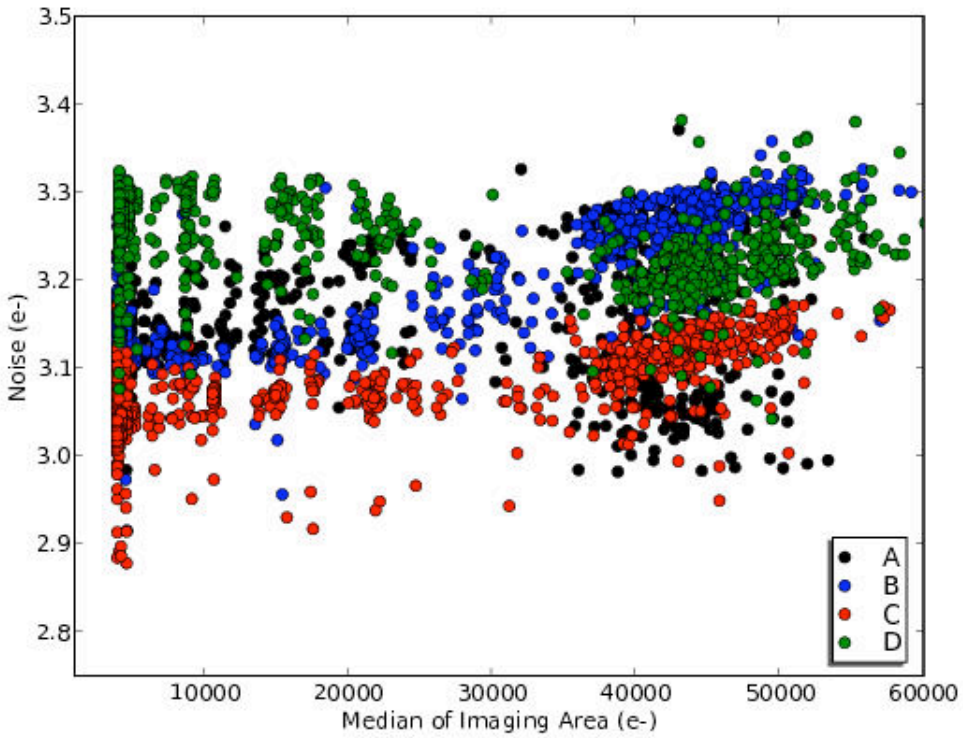

Figure 5 : The read noise is plotted against the median level of the imaging area for each amplifier at -82 C.

1.5 Superbias Frame at -82 C for UVIS-1′

The above discussion has focused nearly entirely on the noise extracted from the imaging and oversan areas of bias frames and so it is only natural that we look more closely at the 2-dimensional structure of these frames. For each MEB, a superbias was created by combining the individual frames (about 60 per MEB) with the 'imcombine' task in PyRAF and the 'average' and 'crrej' options. The result for MEB1 is shown in Fig. 6. The most striking features are the vertical, diffuse bars along the edge of each quadrant, like those seen in the UVIS-2 bias frames (Martel 2007). These bands are due to the luminescence of the protection diodes during the CCD readout. They are likely present in all frames and at similar intensities independent of the exposure time (A. Waczynski, private communication). They are most prominent in the CD chip (bottom). A horizontal slice reveals that the counts rise smoothly and continuously from the center of each chip and peak at column ~230 on the left AC edge and at column ~3830 on the right BD edge. In quadrant D, the mean level at the center of the imaging area is ~0.035 DN while the vertical band peaks at 0.45 DN, more than a factor of ten greater.

Unlike the UVIS-2 detector, there is no odd/even column effect in the quadrant B of the UVIS-1′ superbias for either MEB and so no modifications are required to the 'calwf3' overscan subtraction algorithm. The absence of this effect is also confirmed by S. Baggett (priv. comm.), who reduced the data independently.

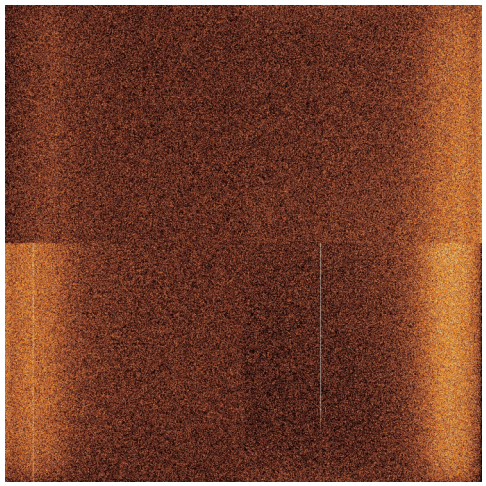

Figure 6 : The superbias frame for MEB1 at -82 C (ABCD, gain=1.5, 1x1).
The overscan regions have been trimmed.

1.6 Contract-End-Item (CEI) Specifications for UVIS-1′

Some pertinent CEI specifications can be addressed with the measurements in this ISR, specifically those that focus on noise levels and repeatability for the unbinned full frames in standard four-amplifier readout mode, a gain of 1.5 e^-/DN, and an operating temperature of -82 C. As mentioned in section 1.2, the CEI specification 4.6.3 of a read noise less than 4 e^- is satisfied for temperatures colder than about -20 C (but the goal of 3 e^- is not). The specification 4.6.14 can also be verified : (1) "UVIS CCD Detector Bias Stability: The detector bias (zero) level over a single row shall be repeatable, during array readout, to at least 2 electrons RMS." (2) "UVIS CCD Detector Bias Correctability: The bias level for the entire array shall be correctable to at least 1 electron RMS."

The repeatability can be verified by measuring the residual levels along rows of pairwise-subtracted bias frames. This is essentially how the noise was measured in the imaging areas but by using the standard deviations. The correctability can be verified in essentially the same manner by subtracting (or correcting) a bias frame with another and then calculating the level of the residual image. We consider each quadrant individually.

Histograms of the average of the residual levels along the rows and for the entire quadrants are all centered on a null value of zero with typical spreads of less than 0.5 e^-. Hence, the bias frames are easily repeatable and correctable within 1 e^- in all four quadrants. Similar results are found for the residuals along the columns.

2. IR

2.1 CDS Noise and Trends at 144 K

In Fig. 7, the CDS noise for the SPARS25 sampling sequence is plotted as a function of the day in the TV3 campaign (Fig. 7). There is a clear and remarkable difference in the noise between MEB1 and MEB2. In quadrants 2, 3, and 4, where the quadrants are labeled counter-clockwise and quadrant 1 is at the top-left, the noise on MEB2 is significantly lower than on MEB1. This behavior is reinforced in Fig. 8, where histograms of the noise are plotted - the distributions are double-peaked for quadrants 2, 3, and 4. The same behavior is observed for the RAPID sampling sequence, but less dramatically because of the smaller number of data points.

The CDS noise can be estimated by fitting the peaks of the histograms - the results are tabulated in Table 2. For both sequences, quadrant 4 shows the most substantial difference between MEBs, about 0.8 e^-. On MEB1, quadrant 4 is the noisiest but on MEB2, it is quadrant 1. We note that the variations in noise can not be due to changes in the FPA temperature; the temperature (monitored by the keyword IRFPATMP) was actually higher by ~1.7K in the MEB2 period at day 100 than in the MEB1 period at day 75. The operation of WFC3 on MEB2 in orbit will therefore minimize the noise in the IR observations, at least for these two sequences.

Our results can be compared with those of Hilbert (2008b). Our absolute noise values are consistently 1 e^- lower than his values (see his Table 2). Although we share the same basic method of calculating the CDS noise by differencing reads up the sampling sequence, we differ in the final binning and histogram fittting, and this may account for this offset (for example, the CDS noise is not calculated as a median in our method). But the relative behavior of the noise between quadrants and MEBs is nearly identical i.e. a lower noise on MEB2 by the same amount.

Table 2 : CDS Noise of the IR-4 Detector in Standard Readout Mode at 144 K

Sequence-MEB	**Quad 1**	**Quad 2**	**Quad 3**	**Quad 4**
RAPID-1	19.31 ± 0.11	19.37 ± 0.12	19.16 ±0.07	19.88 ± 0.09
RAPID-2	19.31 ± 0.11	18.79 ± 0.11	18.84 ± 0.08	19.14 ± 0.08
SPARS25-1	19.73 ± 0.11	19.76 ± 0.11	19.55 ± 0.08	20.34 ± 0.12
SPARS25-2	19.73 ± 0.11	19.25 ± 0.08	19.29 ± 0.06	19.49 ± 0.10

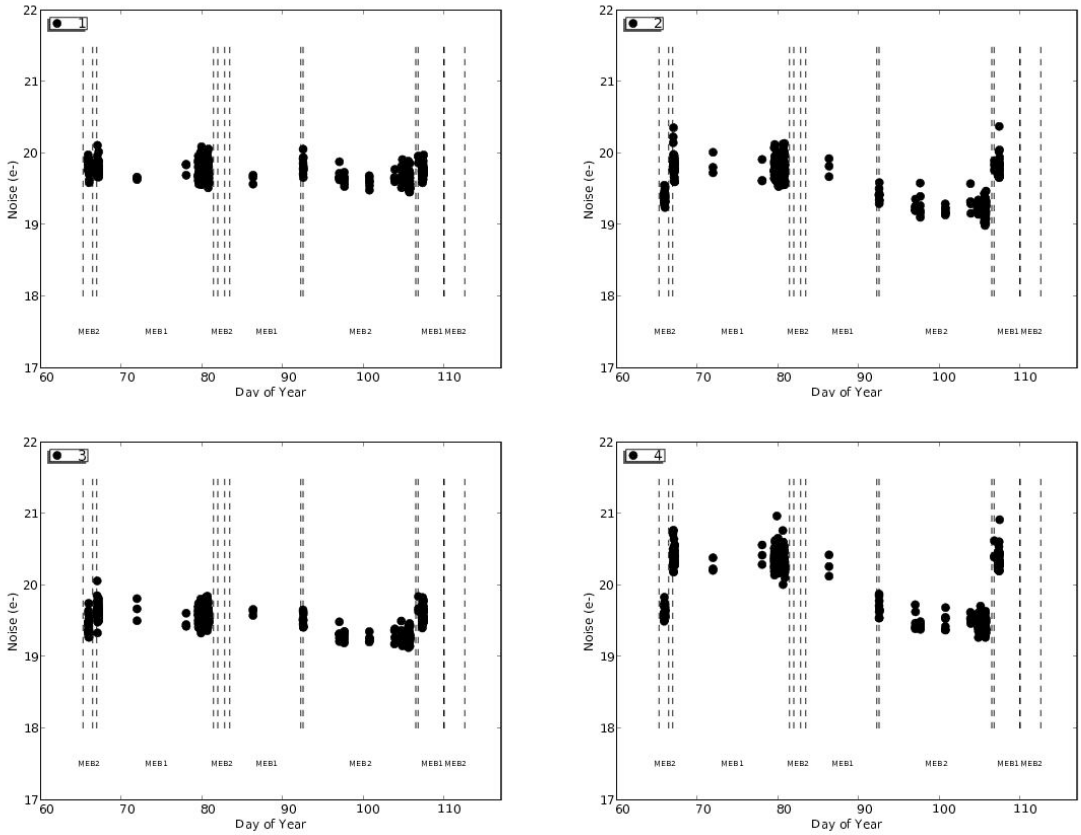

Figure 7 : CDS noise in e^- of the four quadrants of IR-4 for the SPARS25 sequence throughout TV3.

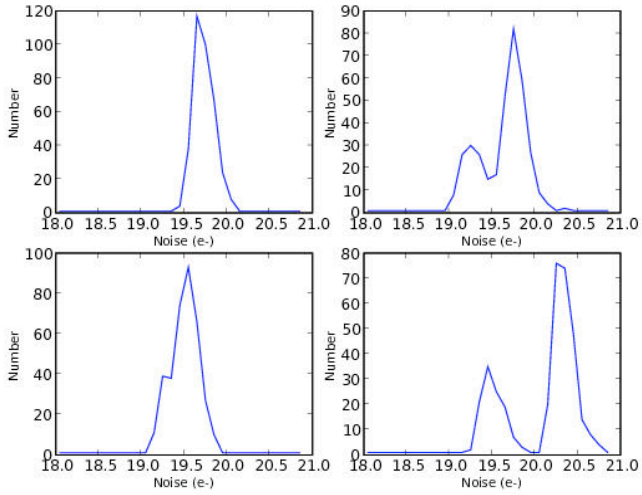

Figure 8 : Histograms of the CDS noise shown in Fig. 7.

Conclusions

We have characterized the read noise of the flight UVIS-1′ and IR-4 detectors of WFC3 using several hundred frames acquired in TV3. For the UVIS, a read noise of ~3.1 e^- is measured for the standard on-orbit configuration. Pairwise subtraction of the imaging area of the bias frames is preferable to the virtual overscan regions in estimating the read noise. The noise is slightly larger for binnings of 2x2 and 3x3. For the IR, the CDS noise is distinctly lower on MEB2 than on MEB1, up to 0.8 e^- for quadrant 4. The operation of WFC3 on MEB2 in orbit will therefore minimize the noise in the IR channel.

References

Baggett, S. 2007, ISR 2007-15: WFC3 Ambient-2 Testing: UVIS Readnoise

Baggett, S. 2008, ISR 2008-13: WFC3 TV3 Testing: UVIS-1′ Gain Results

Baggett, S. & Hilbert, B. 2004, ISR 2004-01: Readnoise and Dark Current in WFC3 Flight CCD Ambient Data

Hilbert, B. 2005, ISR 2005-15, Results of WFC3 Thermal Vacuum Testing - IR Channel Readnoise

Hilbert, B. 2008a, ISR 2008-04, WFC3 TV2 Testing : IR Channel Read Noise

Hilbert, B. 2008b, ISR 2008-25, WFC3 TV3 Testing : IR Channel Read Noise

Hilbert, B. & Baggett, S. 2004, ISR 2004-13: WFC3 UVIS Dark Current and Readnoise from Ambient Testing

Hilbert, B. & Baggett, S. 2005, ISR 2005-13: Results of WFC3 Thermal Vacuum Testing - UVIS Readnoise and Dark Current

Martel, A.R. 2007, ISR 2007-27: WFC3 TV2 Testing: UVIS-2 Read Noise

Martel, A.R. 2008, ISR 2008-02: Python Quick-Look Utilities for Ground WFC3 Images

Robberto, M. 2007a, ISR 2007-12, Analysis of the Sampling Schemes for WFC3-IR

Robberto, M. 2007b, ISR 2007-13: UVIS CCD EPER CTE Measurements in the April 2007 Ambient Calibration Campaign